

Appendix A: Miscellaneous Derivations

A.1 Bending Angle and Bouguer's Law, Eq. (2.2-2)

In geometric optics, a ray, if it exists, must be a path of stationary phase. This is Fermat's principle. In other words, the cumulative phase along the path integral between the positions A and B,

$$\varphi = k \int_A^B n ds = k \int_A^B n \sqrt{1 + (r\theta')^2} dr \quad (\text{A-1})$$

must be stationary with respect to all neighboring paths passing through the end points A and B.¹ Here φ is the phase accumulation along the path; $n = n(r, \theta)$ is the index of refraction; s is path length; and $\theta' = d\theta / dr$, which gives the slope of the ray path. The term "all neighboring paths" means all continuous paths within some suitably defined local region about the actual ray path. Fermat's principle is a local condition, not a global one. From the Calculus of Variations a necessary condition for stationarity is that the ray at all points must

¹ Here we have assumed a Euclidian metric for space-time curvature. In practice, however, with the precise calculation of the predicted phase to be compared with actual data, general relativistic space-time curvature from the mass of the Earth and special relativistic effects from the motions of the satellites have to be accounted for to achieve satisfactory accuracy. The path integral for the ray in this case involves a general relativistic curvature tensor, and the integral is better written in a four-dimensional parametric form. A ray is a geodesic in relativistic four-dimensional space-time. In practice, relativity effects usually are included as small differential corrections to the Euclidian form for the phase delay. They sometimes are referred to as "post-Newtonian" corrections [4].

satisfy Euler's differential equation or its integral equivalent at points of discontinuity in n [1–3]. Euler's equation in polar coordinates is given by

$$\frac{d}{dr} \frac{\partial}{\partial \theta'} \left(n \sqrt{1 + (r\theta')^2} \right) - \frac{\partial}{\partial \theta} \left(n \sqrt{1 + (r\theta')^2} \right) = 0 \quad (\text{A-2})$$

When n is a function of r only, one can integrate Eq. (A-2) to obtain

$$\frac{\partial}{\partial \theta'} \left(n \sqrt{1 + (r\theta')^2} \right) = \text{constant} = a \quad (\text{A-3})$$

Carrying out the differentiation, one obtains

$$\frac{nr^2\theta'}{\sqrt{1 + (r\theta')^2}} = nr \sin \gamma = a = r_* n(r_*) \quad (\text{A-4a})$$

$$\frac{d\theta}{dr} = \pm \frac{a}{r} \frac{1}{\sqrt{n^2 r^2 - a^2}} \quad (\text{A-4b})$$

where γ is the angle between the radius vector and the direction of propagation of the ray at the point (r, θ) (see Fig. A-1). When we set the occulted GPS satellite infinitely afar in the direction $\theta = \pi$, then $\gamma = \theta + \tilde{\alpha}$, where $\tilde{\alpha}$ is the cumulative bending angle of the ray at the point (r, θ) relative to its asymptotic direction prior to encountering the atmosphere. Equation (A-4a) is Bouguer's law, and a is the impact parameter, which is a ray-specific constant when spherical symmetry applies. In Eq. (A-4b), the minus sign is used in the first quadrant and the plus sign in the second quadrant. At the turning point(s) where $d\theta/dr \rightarrow \infty$, it follows that $a = r_* n(r_*)$, where r_* denotes a turning point.

To obtain a differential equation for the bending angle, we note that a small incremental change in position Δs along the ray results in a small incremental

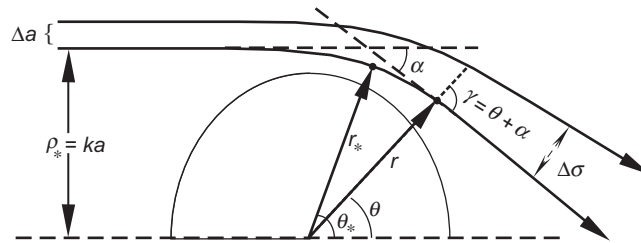


Fig. A-1. Defocusing geometry. Small cross-track displacement Δa of the ray in the plane of propagation before encountering the atmosphere results in a post-encounter cross-track displacement $\Delta \sigma$.

change $\Delta\gamma$ in the angle between the radius vector and the ray path tangent vector. But $\Delta\gamma = \Delta\theta + \Delta\tilde{\alpha}$, even when the occulted Global Positioning System (GPS) satellite is only a finite distance away. By differentiating Bouguer's law, $nr \sin \gamma = a$, with respect to r , replacing $d\gamma/dr$ with $d\theta/dr + d\tilde{\alpha}/dr$, and using Eq. (A-4b) for $d\theta/dr$, one obtains

$$\frac{d\tilde{\alpha}}{dr} = -a \frac{n'}{n} \frac{1}{\sqrt{n^2 r^2 - a^2}} \quad (\text{A-5})$$

Integrating Eq. (A-5) to infinity along both sides of the turning point yields Eq. (2.2-2).

We note from Eq. (A-4b) that a necessary condition for a real solution to Euler's equation and, therefore, for the existence of a ray between specified endpoints, is that $nr \geq a$ at all points along the ray.

A.2 Defocusing

The defocusing factor may be obtained by differentiating the equation for Bouguer's law with respect to a . We assume that the low Earth orbiting (LEO) satellite is located at the point (r, θ) , which is outside of the refracting medium so that $n \equiv 1$ in this neighborhood. Let σ be a cross-track distance perpendicular to the ray at the point (r, θ) . To compute the defocusing, we need the ratio of the signal flux densities for incoming and outgoing rays. Therefore, we need the ratio $\Delta a / \Delta \sigma$, where $\Delta \sigma$ is the displacement of the ray in the cross-direction at the point (r, θ) due to a displacement of the incoming ray at a point before encountering the atmosphere, which is a change in impact parameter Δa (see Fig. A-1). Upon differentiating $nr \sin \gamma = a$ with respect to a while constraining the LEO to lie on the cross-track perpendicular to the ray ($\Delta r = \Delta \sigma \sin \gamma$, $r \Delta \theta = \Delta \sigma \cos \gamma$), we obtain

$$\frac{d\sigma}{da} = 1 - r \cos \gamma \frac{d\alpha}{da} \quad (\text{A-6})$$

But $r \cos \gamma = \sqrt{r^2 - a^2} = D$, which is essentially the distance of the LEO from the Earth's limb minus a relatively small arc length $a\alpha$. Hence,

$$\zeta = \frac{da}{d\sigma} = \left(1 - D \frac{d\alpha}{da}\right)^{-1} \quad (\text{A-7})$$

A.3 Excess Doppler

When one removes the Doppler shift on the measured carrier frequency due to the relative motion between the LEO and the occulted GPS satellite, the remainder due to refraction is called the “excess Doppler.” This is equivalent to removing the relative velocity component along the LEO–GPS line, leaving only the cross-velocity component. The component of the cross-velocity lying in the plane of propagation, that is, the plane containing the GPS–LEO line and the geocenter (assuming spherical symmetry and, therefore, coplanar propagation), is designated as V_{\perp} . Thus, V_{\perp} is the geocentric closing velocity of the turning point or tangency point of the GPS–LEO straight line. For a LEO orbit radius of $1.1R_E$, $V_{\perp} \approx 2.5$ km/s during an occultation through the atmosphere. The exact value differs depending primarily on the angle between V_{\perp} and the orbital cross-velocity vector. When this angle is less than 30 deg, V_{\perp} ranges roughly between 2 and 3 km/s. V_{\perp} is shown pictorially in Fig. A-2, which also shows pre- and post-encounter planar wave fronts of the ray. (Here, the GPS satellite is assumed to be infinitely afar.)

Here is a heuristic derivation of the excess Doppler expressed in terms of bending angle. To eliminate the Doppler shift from the relative velocity between the LEO and the occulted GPS satellite, we freeze the motion of the wave fronts of the signal and consider only the motion of the LEO perpendicular to the approaching wave fronts. Referring to Fig. A-2, we see that a small displacement $V_{\perp}\Delta t$ of the LEO perpendicular to the GPS–LEO line in a short time interval, Δt , results in a change in measured phase at the LEO of

$$\Delta\phi = kV_{\perp}\Delta t \sin\alpha \quad (\text{A-8})$$

By dividing $\Delta\phi$ by $k\Delta t$ and letting $\Delta t \rightarrow 0$, one obtains the excess observed Doppler f_D in hertz. It is related to the observed bending angle through the near-linear expression

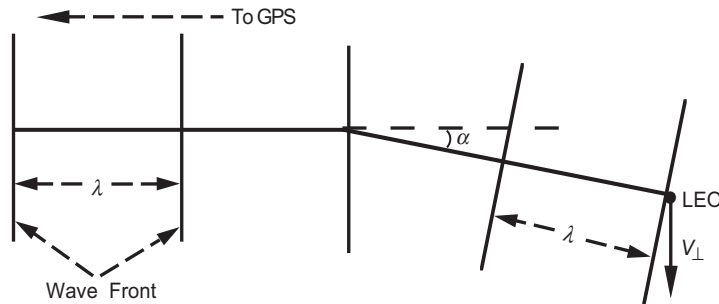


Fig. A-2. Geometry for the relationship between excess Doppler f_D and bending angle α . To first order, $\lambda f_D \doteq \alpha V_{\perp}$.

$$\lambda f_D = \alpha V_{\perp} + O[\alpha^2] \quad (\text{A-9})$$

For dry air at sea level, α is about 20 mrad. Thus, the excess Doppler from dry air ranges up to a few hundred hertz. The Doppler from the relative motion between the two satellites ranges up to 35 kHz.

A more comprehensive version of this expression in Eq. (A-9) can be derived using the transversality condition from the Calculus of Variations [3,5]. The transversality condition results from considering the given ray passing through the positions of the GPS and LEO satellites as being embedded in a family of neighboring rays generated by varying the values of one or more boundary conditions, such as the position coordinates of the LEO and GPS satellites. The phase delay, which is stationary on each ray, then becomes a field variable, in this case a function of the six satellite position coordinates. Displacement of the GPS and LEO satellites over a short time interval Δt to new nearby positions causes a new ray to intersect the new points. The phase delay on the new ray between the new positions of the two satellites minus the phase delay on the old ray between the old positions, $\delta\phi$, is given from the transversality condition. Let

$$F(r, \theta, \theta') = n(r)(1 + r^2\theta'^2)^{1/2} \quad (\text{A-10})$$

which is the integrand in Eq. (A-1) for the path integral giving the phase delay ϕ . The transversality condition gives the change in ϕ resulting from small displacements in the end point positions A and B of the integral in Eq. (A-1) *when the integral is evaluated along a path that gives it a stationary value*. Thus, the path between A and B must satisfy the Euler equation

$$\frac{d}{dr} \left(\frac{\partial F}{\partial \theta'} \right) - \frac{\partial F}{\partial \theta} = 0 \quad (\text{A-11})$$

at every point, or its integral equivalent. By varying the end points, it can be shown from the calculus of variations that the change in ϕ is given from the transversality condition by²

² The transversality condition is related to the Hamilton–Jacobi partial differential equation, which describes the behavior of ϕ as a field variable, that is, as a function of (r, θ) at the end points. To keep the matter simpler, we consider only the variability of ϕ at the single end point at B. We define the conjugate momentum as $p = \partial F / \partial \theta'$, and also the Hamiltonian as $H(r, \theta, \theta') = F - \theta' \partial F / \partial \theta'$. Then in terms of r , p , and θ , it follows that $r\theta' = p / (n^2 r^2 - p^2)^{1/2}$ and the Hamiltonian becomes $r\mathcal{H}(r, \theta, p) = (n^2 r^2 - p^2)^{1/2}$. A specific ray path in the field is described by a pair of first-order differential equations in terms of the independent variable r :

$$\delta\varphi = \left[\left(F - \theta' \frac{\partial F}{\partial \theta'} \right) \delta r + \frac{\partial F}{\partial \theta'} \delta \theta \right]_A^B \quad (\text{A-12})$$

where δr and $\delta \theta$ are the variations in end point values. Upon setting $\delta r = \dot{r} \Delta t$ and $\delta \theta = \dot{\theta} \Delta t$, we obtain

$$\delta\varphi = k(n_L \mathbf{T}_L \cdot \mathbf{V}_L - n_G \mathbf{T}_G \cdot \mathbf{V}_G) \Delta t \quad (\text{A-13})$$

where n is the index of refraction, \mathbf{V} is the velocity vector of the satellite, and \mathbf{T} is the unit tangent vector of the ray. The subscript “L” on these quantities denotes their evaluation at the position of the LEO at the time of reception of the signal, and the subscript “G” denotes evaluation at the occulted GPS

$d\theta/dr = -\partial \mathcal{H} / \partial p$ and $dp/dr = \partial \mathcal{H} / \partial \theta \equiv 0$. The conjugate momentum $p = nr \sin \gamma$ is the impact parameter, and it is a constant along a ray when spherical symmetry applies. But it, along with r and θ , are field variables in Hamilton–Jacobi theory. Also, the Hamiltonian is given by $r\mathcal{H} = nr \cos \gamma$, which is essentially the limb distance minus the small bending-angle offset α . Hamilton–Jacobi theory is the basis for the canonical transform technique in ray theory [6] for converting spatial coordinates for rays (r, θ) into phase space, or canonical coordinates (r, θ, p) . In spatial coordinates, multiple rays may pass through a point (r, θ) in multipath situations, that is, different values of θ' can hold. But, in canonical coordinates, only a single ray can pass through a given point (r, θ, p) , provided that spherical symmetry holds (and super-refracting situations are avoided). One uses a Fourier integral transform similar to the diffraction integral given in Eq. (A-22) to transform the phase and amplitude measurements made by the LEO along a path in spatial coordinates into an equivalent single-valued set in canonical coordinates to obtain the phase and amplitude as a function of p . One then can apply the Abel transform to the derived bending-angle profile in the canonical surface to recover the refractivity profile.

From the transversality condition, it also follows that the behavior of φ as a field variable evaluated at the end point (r, θ) at B is given by $\partial\varphi/\partial r - \mathcal{H} = 0$ and $\partial\varphi/\partial\theta - p = 0$. Upon replacing p by $\partial\varphi/\partial\theta$ in the Hamilton–Jacobi equation, $\partial\varphi/\partial r - \mathcal{H}(r, \theta, p) = 0$, we have $(\partial\varphi/\partial r)^2 + r^{-2}(\partial\varphi/\partial\theta)^2 = |\nabla\varphi|^2 = n^2$, which is the eikonal equation.

satellite at the time of transmission.³ Because φ is stationary on each ray, $\delta\varphi$ depends to first order only on the end point values, which is somewhat remarkable considering that the value of φ comes from a path integral that explicitly accounts for the refractivity along the entire ray path. From $\delta\varphi$, we subtract the term $k\dot{r}_{LG}\Delta t = k\Delta t(\mathbf{V}_L - \mathbf{V}_G) \cdot (\mathbf{r}_L - \mathbf{r}_G) / |\mathbf{r}_L - \mathbf{r}_G|$, which is the phase change from the radial velocity between the two satellites over the time interval Δt . Then dividing by $k\Delta t$ and letting $\Delta t \rightarrow 0$ yields $f_D = (d\varphi / dt) / 2\pi$, the excess Doppler from the intervening medium, which is given by

$$\lambda f_D = n_L \mathbf{T}_L \cdot \mathbf{V}_L - n_G \mathbf{T}_G \cdot \mathbf{V}_G - \frac{(\mathbf{V}_L - \mathbf{V}_G) \cdot (\mathbf{r}_L - \mathbf{r}_G)}{|\mathbf{r}_L - \mathbf{r}_G|} \quad (\text{A-14})$$

This form in Eq. (A-14) accounts for the velocities of both the transmitting and receiving satellites. It is quite general, applying to three-dimensional situations, to finite satellite distances, and to the case where the satellites are located in a refracting medium with or without spherical symmetry.

From Fig. A-3, we obtain a geometric representation of Eq. (A-14). Figure A-3 applies to a coplanar, spherical symmetric geometry. Here triangle OLG defines the instantaneous plane of propagation of the ray from the occulted GPS satellite to the LEO. This plane osculates with time depending on the three-dimensional orientation of the satellite orbit planes and on the satellite orbital positions. The interior angles of this triangle OLG, χ_L , χ_G , and $\theta_G - \theta_L$, and its sides, r_L , r_G , and r_{LG} , are completely determined from the precision orbit determination (POD) information about the orbits of the LEO and the occulted GPS satellite. The refraction-related quantities, which are the impact parameter a and the bending angle $\alpha = \delta_L + \delta_G$, are to be determined from the excess Doppler measurement. From Fig. A-3, the ray path tangent vectors are given by $\mathbf{T}_L = \hat{\mathbf{r}}_L \cos \gamma_L - \hat{\boldsymbol{\theta}}_L \sin \gamma_L$ and $\mathbf{T}_G = -\hat{\mathbf{r}}_G \cos \gamma_G - \hat{\boldsymbol{\theta}}_G \sin \gamma_G$, where $\gamma = \chi + \delta$. Also, $\mathbf{V}_L = \dot{\mathbf{r}}_L \hat{\mathbf{r}}_L + \dot{\boldsymbol{\theta}}_L r_L \hat{\boldsymbol{\theta}}_L$ and $\mathbf{V}_G = \dot{\mathbf{r}}_G \hat{\mathbf{r}}_G + \dot{\boldsymbol{\theta}}_G r_G \hat{\boldsymbol{\theta}}_G$. Here \dot{r} and

³ Besides accounting for light-time effects from the finite speed of light, one also would have to distinguish in a special relativistic framework [4] between the proper time intervals, $\Delta\tau_L$ and $\Delta\tau_G$, kept by the clocks onboard the moving satellites, and the coordinate time interval, Δt , kept in the stationary coordinate frame center assumed here (at position O in Fig. A-3). The transmitted and received carrier frequencies depend on proper time. The differences between these time intervals, and also the difference between the relativistic expression and the classical form for the Doppler shift used to obtain Eq. (A-14), can be expressed as a power series of quadratic and higher powers of (V/c) . Here V is the velocity of the satellite and c is the speed of light. The magnitude of (V/c) is 10 to 25 parts per million. It turns out that because of term cancellation the form given in Eq. (A-14) is relativistically accurate, at least through quadratic terms in (V/c) .

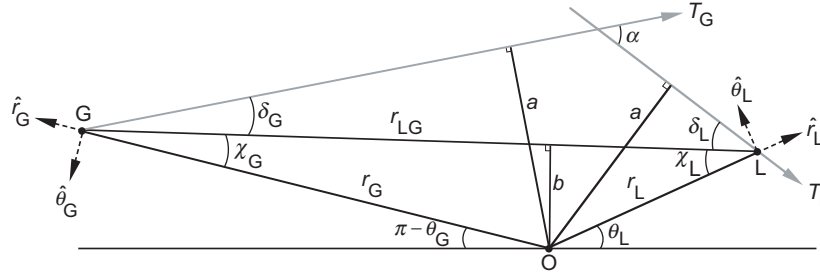


Fig. A-3. Ray path geometry from point G to point L in the plane of propagation for a spherical symmetric medium.

$r\dot{\theta}$ are the radial and transverse components of the orbital velocity vector projected into the plane of propagation defined by the triangle OLG. Also, \hat{r} and $\hat{\theta}$ are orthogonal unit vectors defining the local rotating coordinate frame. The radial velocity between the satellites \dot{r}_{LG} is given by $\dot{r}_{LG} = \dot{r}_L \cos \chi_L + \dot{r}_G \cos \chi_G + b(\dot{\theta}_G - \dot{\theta}_L)$, where b is the impact parameter of the straight line between the LEO and the occulted GPS satellite. In practice, $\dot{\theta}_L$ is roughly an order of magnitude larger than $\dot{\theta}_G$. Also, for near-circular orbits, $r\dot{\theta} \gg \dot{r}$.

By using these geometric expressions and applying Bouguer's law, $a = nr \sin \gamma = \text{constant}$, one obtains from Eq. (A-14) (with $n \equiv 1$)

$$\lambda f_D = \left(\sqrt{r_L^2 - a^2} - \sqrt{r_L^2 - b^2} \right) \frac{\dot{r}_L}{r_L} - \left(\sqrt{r_G^2 - a^2} - \sqrt{r_G^2 - b^2} \right) \frac{\dot{r}_G}{r_G} + (a - b)(\dot{\theta}_G - \dot{\theta}_L) \quad (\text{A-15})$$

The only quantity on the right-hand side (RHS) of Eq. (A-15) not known from POD information is the impact parameter a . Therefore, the measurement of the excess Doppler f_D enables a determination of a . Also, from Bouguer's law we have

$$\left. \begin{aligned} a &= r_L \sin(\delta_L + \chi_L) \\ a &= r_G \sin(\delta_G + \chi_G) \\ \alpha &= \delta_L + \delta_G \rightarrow \alpha \end{aligned} \right\} \rightarrow \delta_L, \delta_G \quad (\text{A-16})$$

from which a determination of the bending angle α follows.

If spherical symmetry does not apply, then these expressions in Eqs. (A-15) and (A-16) become somewhat more complicated, and Bouguer's law does not

apply. Here some recursive ray-tracing technique is required to obtain the turning point position of the ray (r_*, θ_*) and its bending angle. Equation (A-14) shows that the one-to-one relationship between bending angle and excess Doppler still holds, but the relationship between bending angle and turning point must be qualified when spherical symmetry does not apply. In other words, one can conjure up a strong along-track refractive gradient scenario that leads to another turning point value yielding the same bending angle, whereas a gradual departure from spherical symmetry, for example, an oblate spheroid, may not. Figure A-4 shows this former point in a thin phase screen context. Here the limb distance D , or distance of the LEO from the screen, varies with altitude. The same bending angle occurs at two different altitudes in the screen, or at two different impact parameter values.

In Eqs. (A-8) and (A-9), we have simplified the matter further by placing the occulted GPS satellite infinitely afar in the $\theta = \pi$ direction, and we have used the reduced limb distance D to compensate for this simplification. In this case, we set $\mathbf{T}_G = (\mathbf{r}_L - \mathbf{r}_G) / |\mathbf{r}_L - \mathbf{r}_G| \rightarrow -\hat{\mathbf{r}}_G$, $\mathbf{V}_G = 0$, $\chi_G = 0$, and $\delta_G = 0$. Also, $\mathbf{T}_L = \hat{\mathbf{r}}_L \cos \gamma_L - \hat{\theta}_L \sin \gamma_L$, where in this case $\gamma_L = \theta_L + \alpha$. Equation (A-14) becomes

$$\lambda f_D = (\mathbf{T}_L - \mathbf{T}_G) \cdot \mathbf{V}_L = V_{\perp} \alpha + O[\alpha^2] \tag{A-17}$$

where $V_{\perp} = \mathbf{V}_L \cdot \mathbf{T}_{\perp} = -\dot{r}_L \sin \theta_L - r_L \dot{\theta}_L \cos \theta_L$. Equation (A-17) yields the same relationship between excess Doppler and bending angle that is given in Eq. (A-9). For a rising occultation, $\dot{\theta}_L > 0$, and for a setting occultation, $\dot{\theta}_L < 0$.

We note that in the case where r_G is finite, as shown in Fig. A-3, the generalized version of Eq. (A-17) is given by

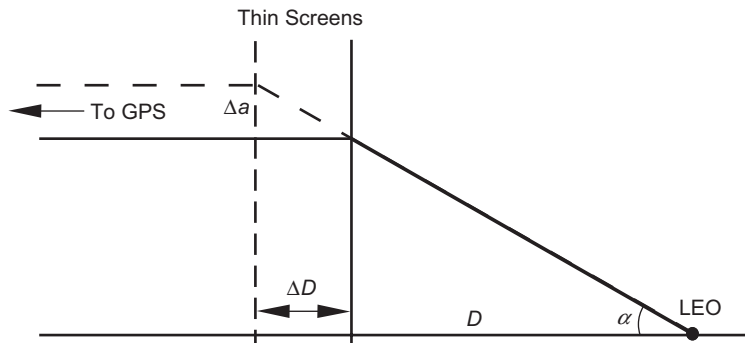


Fig. A-4. Altitude-dependent thin-screen geometry. Because of the assumed horizontal variability in refractivity, the limb distance D is a function of the altitude of the ray path turning point.

$$\lambda f_D = \mathbf{T}_\perp \cdot (\mathbf{V}_L \delta_L - \mathbf{V}_G \delta_G) + \mathcal{O}[\delta_L^2, \delta_G^2] \quad (\text{A-18})$$

where $\mathbf{T}_\perp = -\hat{\mathbf{r}}_L \sin \chi_L - \hat{\boldsymbol{\theta}}_L \cos \chi_L = -\hat{\mathbf{r}}_G \sin \chi_G + \hat{\boldsymbol{\theta}}_G \cos \chi_G$, which is the unit vector in the plane of propagation perpendicular to the straight line between the LEO and the occulted GPS satellite.

Finally, we define \mathbf{a} to be the vector version of the impact parameter directed perpendicular to the plane of propagation. Thus, \mathbf{a} is analogous to the angular momentum vector in classical mechanics. From Eq. (A-4b), it follows that $\mathbf{a} = n(\mathbf{T} \times \mathbf{r})$, which is a constant vector along a specific ray. The satellite positions evolve with time, and different rays intersect those evolving positions. These rays have different values for the impact parameter and bending angle. At the LEO, we set $n_L \equiv 1$. Then differentiating the expression $\mathbf{a} = \mathbf{T}_L \times \mathbf{r}_L$ with respect to time, one obtains $\dot{\mathbf{a}} = \zeta(\mathbf{T}_L \times \mathbf{V}_L)$ for the rate of change of the impact parameter. Also, $\dot{\alpha} = \pm \zeta(d\alpha/da)|\mathbf{T}_L \times \mathbf{V}_L|$, with the plus sign for a rising occultation and the negative sign for a setting occultation. Note that the defocusing factor appears in these expressions for $\dot{\mathbf{a}}$ and $\dot{\alpha}$, and through Eq. (A-7) the defocusing factor also appears in \dot{f}_D . For dry air, $\zeta \approx 0.1$ at sea level. At the tropopause, $\zeta = 0.3 - 0.4$. As a consequence, the variability in f_D resulting from the local variability in the refractivity is increasingly more compressed as the turning point of the ray sinks deeper into the troposphere.

A.4 Scalar Diffraction Theory

Fresnel diffraction effects are computed using scalar diffraction theory. It is based on the Helmholtz–Kirchoff integral theorem from classical electrodynamics, which relates the amplitude and phase distributions of an electromagnetic wave over a surface to the amplitude and phase at a point interior to the surface [7,8]. One form of this integral theorem is given by

$$E(\mathbf{r}_1, t) = \frac{1}{2\pi c} \iint_S \frac{1}{r_{12}} \frac{\partial}{\partial t} E(\mathbf{r}_2, t_R) (\hat{\mathbf{r}}_{12} \cdot \hat{\mathbf{n}}(\mathbf{r}_2)) dS \quad (\text{A-19})$$

Here \mathbf{r}_1 is the position vector from the origin to point 1, where the field is to be evaluated; \mathbf{r}_2 is the position vector to point 2 on the surface element dS ; and $\hat{\mathbf{r}}_{12}$ is a unit vector directed along $\mathbf{r}_{12} = \mathbf{r}_2 - \mathbf{r}_1$. The unit vector $\hat{\mathbf{n}}(\mathbf{r}_2)$ is directed outward along the normal to dS (away from the position \mathbf{r}_1). The quantity t_R is the retarded time, $t_R = t - r_{12}/c$, which accounts for the extra time r_{12}/c required for a wavelet from dS to reach the point at \mathbf{r}_1 . This surface integral is valid when the wavelength of the wave is small compared to the scale of the radiating surface.

Let us assume that we have a harmonic wave with an angular frequency ω . Then

$$E(\mathbf{r}_2, t_R) = E(\mathbf{r}_2) \exp(\pm i\omega t_R) = E(\mathbf{r}_2) \exp(\pm i\omega t) \exp(\mp ikr_{12}) \quad (\text{A-20})$$

where $k = 2\pi / \lambda$, the wave number of the wave in a vacuum. Here, the top or bottom sign to be adopted depends on the propagation sense. Because we assume homogeneity in the transverse horizontal direction, we have coplanar propagation; \mathbf{r}_1 and \mathbf{r}_2 are coplanar and $E(\mathbf{r}_2)$ is invariant in the transverse horizontal direction. Then, the two-dimensional surface integral in Eq. (A-19) may be reduced to a one-dimensional path integral by integrating along the transverse direction. Let C be the path defined by the intersection of the plane of propagation and the radiating surface S . Let y be the displacement perpendicular to the plane of propagation. Let the three-dimensional distance $(r_{12})_{3D}$ be written in terms of the two-dimensional distance $(r_{12})_{2D}$ plus the offset y in the transverse direction. Then using the Fresnel approximation, we have $(r_{12})_{3D} \doteq (r_{12})_{2D} + y^2 / 2(r_{12})_{2D}$, which is valid when $|y|/r_{12} \ll 1$, or, equivalently, when the scale along y from which significant contributions to the integral occur is small compared to r_{12} . For the time-independent part of the wave, Eq. (A-19) becomes

$$E(\mathbf{r}_1) \doteq \frac{\pm i}{\lambda} \int_C \left(\frac{E(\mathbf{r}_2)}{r_{12}} \exp(\mp ikr_{12}) ds \right) \int_{-\infty}^{\infty} (\hat{\mathbf{r}}_{12} \cdot \hat{\mathbf{n}}(\mathbf{r}_2)) \exp\left(\mp ik \frac{y^2}{2r_{12}}\right) dy \quad (\text{A-21})$$

Here $ds = |d\mathbf{r}_2|$ is a line element on the coplanar path C . Also, we have dropped the subscript “2D” denoting a two-dimensional vector. Because the wavelength is very small compared to the scale of the surface, the obliquity term $\hat{\mathbf{r}}_{12} \cdot \hat{\mathbf{n}}(\mathbf{r}_2)$ can be moved out of the transverse integral because the phasor $\exp(iky^2 / 2r_{12})$ winds up so rapidly. The value of this integral in the transverse direction is given by a complete complex Fresnel integral, and it is equal to $(1 \pm i)\sqrt{\lambda r_{12}}$. For the two-dimensional case, Eq. (A-21) becomes, for the time-independent part of the wave,

$$E(\mathbf{r}_1) = \sqrt{\frac{\pm i}{\lambda}} \int_C \left(\frac{E(\mathbf{r}_2)}{r_{12}^{1/2}} \exp(\mp ikr_{12}) (\hat{\mathbf{r}}_{12} \cdot \hat{\mathbf{n}}(\mathbf{r}_2)) \right) ds \quad (\text{A-22})$$

By adopting the top sign in Eq. (A-22), we have the basis for the back plane propagation method used to map the actual LEO observations of phase and amplitude backwards (toward the emitter) to an equivalent set in a virtual plane

close to the limb of the Earth. Multipath in the back plane can be significantly reduced with this technique [9,10].

Adopting the bottom sign in Eq. (A-22) leads directly to the Rayleigh–Sommerfeld scalar diffraction integral introduced in Section 2.5. In a thin-screen model (see Fig. 2-3) where the screen is planar and mounted perpendicular to the GPS–LEO line, we use the Fresnel approximation again, $r_{12} \doteq D + (h - h_{LG})^2 / 2D$, where D is the distance of the LEO from the screen and $h - h_{LG}$ is the vertical offset. Because $D \gg h$, the obliquity term $\hat{r}_{12} \cdot \hat{n}(r_2)$ can be set to unity in our qualitative treatment. Placing these substitutions into Eq. (A-22) and replacing $E(r_2)$ with the thin-screen phase function in Eq. (2.3-16) yields the form for the Rayleigh–Sommerfeld integral given in Eq. (2.5-1).

A.5 The First Fresnel Zone

The definition of the first Fresnel zone is a straightforward byproduct from the Fresnel phase term in the Rayleigh–Sommerfeld integral [Eq. (2.5-1)]. The first Fresnel zone can be defined as a solid angle observed by the LEO or, equivalently, as an area in the thin screen containing all points that produce an observed phase at the LEO that differ from the stationary phase value by π rad or less. The second Fresnel zone contains those points that produce an observed phase that differs from the stationary phase value by π to 2π rad, and so on for higher-order zones. The second- and higher-order zones typically are simply connected and roughly concentric around the first zone. The idea is that the second- and higher-order zones produce radiation at the LEO that largely cancels out through mutual destructive interference, effectively leaving only radiation emanating from the first zone, which more or less arrives in-phase at the LEO. In any case, the first zone contains the stationary phase point as its centroid.

The first Fresnel zone provides a resolution limit for a single observation made by the LEO in a manner similar to the way the Airy disk provides a resolution limit for an optical instrument. Also, the first Fresnel zone provides a threshold index for the presence of diffraction effects. When the transition length of a propagation feature, such as a refraction perturbation, is short compared to the radius of the first Fresnel zone, the feature is called “sharp” and geometric optics tends to become less accurate; diffraction effects usually should be included. On the other hand, if the transition length is long, geometric optics with interference effects from multiple rays may suffice (see Section 2.6 for further discussion).

From the definition given above, we require that the boundary of the first Fresnel zone be defined by the locus of points in h -space that yields the condition on the Fresnel phase function [see Eq. (2.5-1)]

$$\Phi(\tilde{h}, h_{\text{LG}}) - \Phi(h(h_{\text{LG}}), h_{\text{LG}}) = \pi \quad (\text{A-23})$$

where $h(h_{\text{LG}})$ is the stationary phase altitude in the thin screen for a given value of h_{LG} . If we expand Eq. (A-23) in a quadratic Taylor series about the stationary phase altitude, we obtain

$$\frac{1}{2} \frac{\partial^2 \Phi}{\partial h^2} \Big|_{\tilde{h}=h} (\tilde{h} - h(h_{\text{LG}}))^2 = \frac{\pi}{\lambda D} \left(1 - D \frac{d\alpha}{dr} \right)_{\tilde{h}=h} (\tilde{h} - h(h_{\text{LG}}))^2 \doteq \pi \quad (\text{A-24})$$

from which it follows that $\tilde{h} = \mathcal{F}(h(h_{\text{LG}}))$. Thus, the “radius” of the first Fresnel zone is given by

$$\mathcal{F} = \sqrt{\zeta \lambda D} \quad (\text{A-25})$$

where ζ is the defocusing factor given by Eq. (A-7) and evaluated at the stationary phase point determined from $h = h(h_{\text{LG}})$. It follows from this discussion that the first Fresnel zone is an ellipse with a semi-major axis length of $\sqrt{\lambda D}$ and a semi-minor (when $|\zeta| < 1$) axis length of $(\zeta \lambda D)^{1/2}$.

A.6 The Abel Transform

The Abel integral transform has been a data analysis tool in seismology for nearly a century. Under the assumption of spherical symmetry, it is used to recover the radial profile of seismic velocity from propagation delay data taken from seismometer arrays. The first suggestion of its use in a radio occultation is found in [11].

From the Doppler observations of the occulted GPS satellite and the POD information, one obtains the excess Doppler and the relative coordinates and velocities of the LEO and GPS satellites. One converts this information into a bending-angle profile $\alpha(a)$, that is, at each observational epoch one obtains a determined bending-angle value $\hat{\alpha}$ and an impact parameter value \hat{a} , per our discussion earlier on excess Doppler, specifically Eqs. (A-8) through (A-16). One uses this observed profile to form the integral

$$I(a) = \int_a^\infty \frac{\alpha(\xi)}{\sqrt{\xi^2 - a^2}} d\xi \quad (\text{A-26})$$

where $\alpha(\xi)$ is the profile of the bending angle given from the observation sequence $(\hat{\alpha}_\kappa, \hat{a}_\kappa)$, $\kappa = 1, 2, \dots$. Then, using Eq. (2.2-2) for $\alpha(\xi)$ and assuming that $N(\infty) = 0$, it is easily shown that

$$\begin{aligned}
I(a) &= \int_a^\infty \left(-2\xi \int_\xi^\infty \frac{1}{n} \frac{dn}{d\rho} \frac{d\rho}{\sqrt{(\xi^2 - a^2)(\rho^2 - \xi^2)}} \right) d\xi \\
&= -2 \int_a^\infty \frac{1}{n} \frac{dn}{d\rho} d\rho \left(\int_a^\rho \frac{\xi d\xi}{\sqrt{(\xi^2 - a^2)(\rho^2 - \xi^2)}} \right) = \pi \log[n(a)] \doteq \pi N(a)
\end{aligned} \tag{A-27}$$

Thus, $N(a)$ from Eq. (A-27) and $\alpha(a)$ from Eq. (2.2-2') essentially form an Abel Transform pair.

In practice with actual data, α_κ approaches zero as a_κ increases. Therefore, the measured value of α_κ becomes increasingly dominated by measurement noise. Usually the measured profile $\hat{\alpha}_\kappa$ is assisted by use of an a priori atmospheric model at thinning altitudes, for example, above 30 to 40 km.

A.7 Sensitivity of the Recovered Refractivity to an Error Source

Since the Abel transform is a linear operator, it is straightforward to use it to evaluate the sensitivity of the recovered refractivity to an error in the observations from essentially any source, provided that it can be expressed in terms of an equivalent error in the bending-angle profile, and provided that it is indeed sufficiently small that the reference ray path is minimally perturbed. It follows from Eq. (A-27) that the error in the recovered refractivity profile $\delta\hat{N}(a)$ is given in terms of the error profile in bending angle $\delta\alpha(a)$ by

$$\delta\hat{N}(a) = \frac{1}{\pi} \int_a^\infty \frac{\delta\alpha(\xi)}{\sqrt{\xi^2 - a^2}} d\xi \tag{A-28}$$

This expression is valid for a thin medium. However, in general the perturbation in $\alpha(a)$ results in a different ray path being followed, limiting the accuracy of Eq. (A-28). This expression is used in Appendix F on the effect of cycle slips on the recovered refractivity profile.

A.8 Perturbation of the Bending-Angle Profile Near a Boundary

To evaluate Eq. (2.2-2), we will need expressions for $\alpha(r_*)$ and for its sensitivity to changes in the parameters that describe the refractivity profile. Here the sensitivities of $\alpha(r_*)$ to a discontinuous change at $r = r_o$ in scale height and in lapse rate are developed. We will obtain expressions for the change in bending angle while holding the point of tangency of the ray r_* fixed

at $r_* = r_o$. For the isothermal case, when H_{p_o} remains constant throughout the atmosphere, Eq. (2.2-2) becomes

$$\alpha(r_o) = \frac{2aN_o}{H_{p_o}} \int_{r_o}^{\infty} \exp\left(\frac{r_o - r}{H_{p_o}}\right) \frac{dr}{n\sqrt{n^2r^2 - a^2}}, \quad a = r_on(r_o) \quad (\text{A-29})$$

If one makes certain approximations in Eq. (A-29) that are applicable to a thin exponential atmosphere [12], it can be shown that $\alpha(r_o)$ is given by

$$\alpha(r_o) = \sqrt{\frac{2\pi r_o}{H_{p_o}}} N(r_o) ((\sqrt{2} - 1)\beta_o + 0.28\beta_o^2 + \dots) \quad (\text{A-30})$$

where $\beta_o = |n'r/n|_o = N_or_o/H_{p_o}$ is the ratio of the impact parameter of the ray to its radius of curvature. Equation (A-30) is fairly accurate for a thin exponentially distributed atmosphere. The error is less than 1 percent for dry air at sea level. It takes into account bending terms along the ray path to second order in β_o . Equation (A-30) begins to break down when β_o exceeds roughly 0.5. By differentiating Eq. (A-30), one obtains

$$-\frac{H_{p_o}}{\alpha} \frac{\partial \alpha}{\partial H_{p_o}} \triangleq -K_H = \frac{1}{2} + 0.41\beta_o + 0.39\beta_o^2 + \dots \quad (\text{A-31})$$

Equation (A-31) also can be obtained by explicitly differentiating Eq. (A-29) with respect to H_{p_o} and carrying out the required integrations. For example, if one ignores the first- and higher-order terms in β_o , differentiating Eq. (A-29) yields

$$\frac{\partial \alpha}{\partial H_{p_o}} = -\frac{\alpha}{H_{p_o}} + \frac{2r_oN_o}{H_{p_o}^3} \int_{r_o}^{\infty} \exp\left(\frac{r_o - r}{H_{p_o}}\right) \frac{(r - r_o)dr}{n\sqrt{n^2r^2 - a^2}} + O[\beta_o] \frac{\alpha}{H_{p_o}} \quad (\text{A-32})$$

or

$$\frac{\partial \alpha}{\partial H_{p_o}} \doteq -\frac{\alpha}{H_{p_o}} + \frac{1}{H_{p_o}} \sqrt{\frac{2r_o}{H_{p_o}}} N(r_o) \int_{r_o}^{\infty} \sqrt{\frac{(r - r_o)}{H_{p_o}}} \exp\left(\frac{r_o - r}{H_{p_o}}\right) \frac{dr}{H_{p_o}} = -\frac{\alpha}{2H_{p_o}} \quad (\text{A-33})$$

At $r_o - R_E = +10$ km, with $H_{p_o} = 7$ km, and $N_o = N(r_o) = 70 \times 10^{-6}$, Eq. (A-31) gives $K_H \cong -0.53$.

Next, an expression for α is obtained that is an explicit function of the lapse rate, which is assumed to be a constant above $r = r_o$. Let that function be given by $\alpha[\gamma, r]$. We will need to evaluate

$$\frac{\partial \alpha}{\partial \gamma} = -2a \int_{r_o}^{\infty} \frac{\partial}{\partial \gamma} \left[\frac{n'}{n \sqrt{n^2 r^2 - a^2}} \right] dr \quad (\text{A-34})$$

when the refractivity profile has an explicit dependency on the lapse rate. (Here the refractivity at r_o is assumed to be invariant to a change in γ .) From the assumption of hydrostatic equilibrium and use of the perfect gas law, one has

$$\left. \begin{aligned} -\frac{1}{\rho} \frac{d\rho}{dr} &= H_p^{-1} = H_p^{-1} + \gamma \\ H_p^{-1} &= \frac{\mu g}{kT}, \quad \gamma = \frac{1}{T} \frac{dT}{dr} \end{aligned} \right\} \quad (\text{A-35})$$

Here ρ is the mass density of the atmosphere. Let the temperature vary linearly with altitude and be given by

$$T = T_o [1 + \gamma(r - r_o)] \quad (\text{A-36})$$

and γ is assumed to be constant above $r = r_o$. Inserting Eq. (A-36) into Eq. (A-35) and integrating upward from $r = r_o$, one obtains for the density

$$\left. \begin{aligned} \log \left(\frac{\rho}{\rho_o} \right) &= -\frac{1}{\gamma H_{p_o}} \log [1 + \gamma(r - r_o)] \\ H_{p_o}^{-1} &= H_p^{-1} + \gamma \end{aligned} \right\} \quad (\text{A-37})$$

where ρ_o is the density at $r = r_o$. Now, the refractivity at tropopause altitudes and higher is given by

$$N(r) = N_o \frac{\rho(r)}{\rho_o} \quad (\text{A-38})$$

This form for $N(r)$ is used in Eq. (2.2-2), which is expanded to second order in γ . Then, certain approximations are made that are consistent with capturing at least all of the second-order terms in β_o . Therefore, this approach must take into account bending along the ray path of integration, which was also included in the derivation of Eq. (A-30). One replaces the integration variable r with arc

length s in Eq. (2.2-2) and uses the ray path curvature relationship,⁴ expanded to second order in β_o . It can be shown that the integration yields

$$\alpha(r_o, \gamma, H_{p_o}) = \sqrt{\frac{2\pi r_o}{H_{p_o}}} N_o \left[1 + 0.41\beta_o + \frac{3}{8}(\gamma H_{p_o}) + 0.28\beta_o^2 + 0.37\beta_o(\gamma H_{p_o}) - \frac{7}{128}(\gamma H_{p_o})^2 + \dots \right] \quad (\text{A-39})$$

which, with Eqs. (A-37) and (A-38), provides a vertical profile of the bending angle for a constant lapse rate in a dry and spherical symmetric atmosphere that is in hydrostatic equilibrium.

By differentiating Eq. (A-39) with respect to γ , one obtains

$$\begin{aligned} \frac{1}{\alpha H_p} \frac{\partial \alpha}{\partial \gamma} \Big|_{r=r_o} &\triangleq K_\gamma \\ &= \frac{3}{8} + \left(\frac{31\sqrt{2} - 32}{32} \right) \beta_o - \frac{1}{4}(\gamma H_{p_o}) + O[\beta_o, (\gamma H_{p_o})]^2 \end{aligned} \quad (\text{A-40})$$

By differentiating Eq. (A-39) with respect to H_{p_o} , one obtains an improved value for K_H that accounts for a non-zero lapse rate,

$$\frac{H_p}{\alpha} \frac{\partial \alpha}{\partial H_p} \Big|_{r_o} = K_H = -\frac{1}{2} - 0.41\beta_o + \frac{3}{8}\gamma H_{p_o} + O[\beta_o, \gamma H_{p_o}]^2 \quad (\text{A-41})$$

At $r_o - R = 10$ km, one obtains

$$\frac{1}{\alpha H_{p_o}} \frac{\partial \alpha}{\partial \gamma} \Big|_{\gamma=0} = 0.40 \quad (\text{A-42})$$

Although a change in lapse rate at $r = r_o$ does produce an “immediate” change in H_{p_o} and, therefore, in the gradient of the refractivity, the consequent change

⁴ Let $z(x, r_*)$ be the vertical deflection of the ray path from its horizontal tangent line at the turning point. For an exponential refractivity profile, it is given by

$$z(x, r_*) = (\pi)^{1/2} \beta(r_*) H_{p_o} \left(|x| \operatorname{erf}(|x|) - (1 - \exp(-x^2)) / (\pi)^{1/2} \right) + O[\beta^2 H_{p_o}]$$

where x is the normalized arc length from the tangent point, $x = s / (2r_o H_{p_o})^{1/2}$.

in the temperature profile above $r = r_o$ induces a change in the density scale height profile in this regime that has a polarity opposite to that of the incremental change in H_{p_o} . This partially offsets the effect of the initial change in the refractivity gradient at $r = r_o$. Hence, one would expect the smaller value (0.4) for K_γ (for $\gamma = 0$) relative to the value (0.53) for K_H .

A.9 Bending-Angle Perturbation

Approximate expressions for the integrals in Eq. (2.3-20) valid through the zeroth order in β (no ray path bending corrections applied) can be readily obtained through simplifications of the integrands. More accurate expressions valid to higher powers in β and γ also can be obtained, but these calculations, like those carried out in the case of the derivations of Eqs. (A-30) and (A-39), are more tedious. The zeroth-order expressions have been compared with a numerical integration of Eq. (2.3-20) for $\gamma = 0$; good agreement has been obtained for “thin atmosphere” conditions. Here one represents the ray path along which the integrations in Eq. (2.3-20) follow by the straight line approximation:

$$r = r_o + \frac{s^2}{2r_o} \hat{=} r_o + x^2 H_{p_o} \quad (\text{A-43})$$

where s is arc length measured from the point of tangency. The radial integration variable r in Eq. (2.3-20) is replaced by s , and all terms of degree 1 and higher in β are dropped. This is carried out for Cases B and C.

With the simplifications in ray path representation in place, the “+” and “-” integrals in Eq. (2.3-20) each have the form

$$\begin{aligned} I &= -2a^- \int_{r_o}^{\infty} \frac{1}{n} \frac{dn}{dr'} \frac{dr'}{\sqrt{(nr')^2 - (a^-)^2}} \\ &= \sqrt{\frac{8r_o}{H_{p_o}}} N(r_o) [1 + (\gamma H_{p_o})] \int_0^{\infty} \exp(-x^2) \left[1 - (\gamma H_{p_o}) \left(2x^2 - \frac{1}{2}x^4 \right) + O[(\gamma H_{p_o})^2] \right] \frac{xdx}{\sqrt{\sigma^2 + x^2}} \\ &= \sqrt{\frac{2\pi r_o}{H_{p_o}}} N(r_o) \left[F(\sigma) + (\gamma H_{p_o}) \left\{ \left(K_\gamma + \frac{3\sigma^2}{2} + \frac{\sigma^4}{2} \right) F(\sigma) - \frac{1}{\sqrt{\pi}} \left(\frac{5\sigma}{4} + \frac{\sigma^3}{2} \right) \right\} + O[(\gamma H_{p_o})^2] \right] \end{aligned} \quad (\text{A-44})$$

where $F(\sigma)$ is defined by Eq. (2.3-28) and σ is given by Eq. (2.3-26).

For Case B with $\gamma = 0$, Eq. (2.3-20) becomes

$$\alpha(r) \doteq \begin{cases} \alpha^-(r) + \alpha^+(r_o)F(\sigma^+) - \alpha^-(r_o)F(\sigma^-), & r \leq r_o \\ \alpha^+(r), & r > r_o \end{cases} \quad (\text{A-45})$$

where $\sigma^\pm = (h_o - h)/H_{p_o}^\pm$ and $\alpha^\pm(r)$ is given by Eq. (A-25). By expanding Eq. (A-45) in a Taylor series in powers of $[H_{p_o}^+ - H_{p_o}^-]$ and using Eq. (A-39) for $\alpha^+(r_o) - \alpha^-(r_o)$, one obtains Eq. (2.3-30).

For Case C, the quantity H_{p_o} is held fixed and γ is varied. Equation (2.3-31) follows directly from inspecting the coefficient of the (γH_{p_o}) term in Eq. (A-44). Differential expressions for these cases also can be developed that account for the effects of ray path bending. A first-order treatment is given below for Case A.

A.10 Bending-Angle Perturbation by a Discontinuous Refractivity, Case A

Obtaining the change in bending angle when n is discontinuous across a boundary in an otherwise smoothly refracting medium follows a course similar to that followed for Cases B and C. However, in Case A, one also has to account for the discontinuity in the impact parameter a when the ray contacts the boundary at $r = r_o$. This results in the σ_+ term in Eq. (2.3-29). Here one has to account for effects of the different impact parameters that arise in evaluating Eq. (2.3-20): $a^\pm = rn^\pm(r)$.

Both the continuous and discrete form of Snell's law must be applied in the neighborhood across a boundary marking a discontinuity in the index of refraction. Also, accounting for ray path bending will improve the accuracy of the analytic expressions for the overall refractive bending. Ray path bending will alter the intersection point of the ray with the boundary relative to the intersection point that holds for the straight-line assumption. Therefore, both the direction of the local normal to the boundary surface and the direction of the impinging ray are altered by ray path bending. Most of the first-order ray path bending can be accounted for by expanding $z[x, r_o]$, given in Footnote 4, in powers of s . This yields $z = \beta s^2 / 2r_o + O[s^3]$, where z is the departure of the ray from a straight-line path. Accordingly, the amended version of Eq. (A-43) that accounts for first-order bending (most of it) is given by

$$r = r_o + x^2(1 - \beta_o)H_{p_o} \quad (\text{A-46})$$

From this it is easily shown that the change $\Delta\theta$ in the direction of the local normal at the amended intersection point is given to first order by

$$\Delta\theta \doteq \sqrt{\frac{r_o - r}{2r_o}} \frac{\beta_o}{(1 - \beta_o)^{3/2}} \quad (\text{A-47})$$

Also the change in direction of the ray at the intersection point due to ray path bending can be shown to be just $2\Delta\theta$. Thus, the change in angle of incidence on the interior side of the boundary is $\Delta\theta$. The change in bending angle across the boundary due to the discontinuity in refractivity, including first-order ray path bending within the interior of the sphere, is given from Bouguer's law by

$$\Delta\alpha_S(r) = \sin^{-1}\left(\frac{rn^-}{r_on^+}\right) - \sin^{-1}\left(\frac{r}{r_o}\right) - \frac{\Delta N}{n^-} \Delta\theta, \quad r \leq \min\left[r_o, r_o \frac{n^+}{n^-}\right] \quad (\text{A-48})$$

However, $\Delta\theta$ is of the order of a milliradian for the ray tangency point located within a few kilometers of the boundary, and also ΔN is small. Consequently, the last term in Eq. (A-48), which is due to ray path bending, can be ignored for the discrete part of the bending angle.

For the continuous or integral portion of the bending angle, we follow a line similar to that followed for Cases B and C except that we take into account ray path bending. Equation (2.2-2) is a *path* integral, that is, it is assumed implicitly that the integrand is evaluated along the ray path [see Eq. (A-5)]. This means that, when one makes a change of variable from the radial coordinate to path length, one must explicitly include the curvature of the ray path in that relationship. Using Eq.(A-46) to account for the effect of ray path bending, one obtains for the overall change in bending, including the discrete component,

$$\alpha(r) \doteq \begin{cases} \alpha^+(r)e^{-\kappa} \operatorname{erfc}(\sqrt{\sigma^2 - \kappa}) - \alpha^-(r) \operatorname{erf}(\sigma) + \Delta\alpha_S, & r \leq \tilde{r} \leq r_o \\ \alpha^+(r), & r > r_o \end{cases} \quad (\text{A-49})$$

Here $\operatorname{erfc}(x) = 1 - \operatorname{erf}(x)$, $\kappa = -r_o \Delta N / (H_{p_o} (1 - \beta_o))$, and \tilde{r} is the critical reflection radius. Expanding Eq.(A-49) to first order in ΔN and setting $\beta_o = 0$ yields Eq. (2.3-27).

Finally, when the ray lies only in the “+” regime,

$$\alpha(r) = \alpha^+(r), \quad r > r_2 \quad (\text{A-50})$$

A.11 The Fresnel Transform Pair

The Fresnel transform pair is a special case of the two-dimensional scalar diffraction formula given in Eq. (A-22) that is obtained when the Fresnel approximation is used and the integration is along a straight line. It should be

clear that reciprocity applies to the two forms of the scalar diffraction integral given in Eq. (A-22); we can use the top signs to integrate $E(\mathbf{r}_2)$ along the curve C to obtain $E(\mathbf{r}_1)$, or we can use the bottom signs to integrate $E(\mathbf{r}_1)$ along another curve to get $E(\mathbf{r}_2)$. Therefore, these two forms are the inverses of each other.

Similarly, from Eq. (2.10-3), we have for the Rayleigh–Sommerfeld integral, expressed in Fresnel variables, $u = h(2/\lambda D)^{1/2}$ and $u_{\text{LG}} = h_{\text{LG}}(2/\lambda D)^{1/2}$,

$$E(u_{\text{LG}}) \exp(i\psi(u_{\text{LG}})) = \frac{1}{1+i} \int_{-\infty}^{\infty} A(u) \exp\left(i\left(\varphi(u) + \frac{\pi}{2}(u - u_{\text{LG}})^2\right)\right) du \quad (\text{A-51})$$

We multiply the left-hand side (LHS) of Eq. (A-51) by $\exp(-i\pi(\tilde{u} - u_{\text{LG}})^2/2)$ and integrate on u_{LG} to obtain

$$\begin{aligned} & \int_{-\infty}^{\infty} E(u_{\text{LG}}) e^{i\left(\psi(u_{\text{LG}}) - \frac{\pi}{2}(\tilde{u} - u_{\text{LG}})^2\right)} du_{\text{LG}} \\ &= \frac{1}{1+i} \int_{-\infty}^{\infty} \int_{-\infty}^{\infty} A(u) e^{i\left(\varphi(u) + \frac{\pi}{2}(u - u_{\text{LG}})^2 - \frac{\pi}{2}(\tilde{u} - u_{\text{LG}})^2\right)} du du_{\text{LG}} \\ &= \frac{1}{1+i} \int_{-\infty}^{\infty} \left(A(u) e^{i\left(\varphi(u) + \frac{\pi}{2}(u^2 - \tilde{u}^2)\right)} \int_{-\infty}^{\infty} e^{i\pi(\tilde{u} - u)u_{\text{LG}}} du_{\text{LG}} \right) du \\ &= \frac{2}{1+i} \int_{-\infty}^{\infty} A(u) e^{i\left(\varphi(u) + \frac{\pi}{2}(u^2 - \tilde{u}^2)\right)} \delta(\tilde{u} - u) du = \frac{2}{1+i} A(\tilde{u}) e^{i\varphi(\tilde{u})} \end{aligned} \quad (\text{A-52})$$

It follows that

$$A(u) \exp(i\varphi(u)) = \frac{1}{1-i} \int_{-\infty}^{\infty} E(u_{\text{LG}}) \exp\left(i\left(\psi(u_{\text{LG}}) - \frac{\pi}{2}(u - u_{\text{LG}})^2\right)\right) du_{\text{LG}} \quad (\text{A-53})$$

which is Eq.(2.10-4). The Dirac delta function,

$$\delta(x) = \frac{1}{2\pi} \int_{-\infty}^{\infty} \exp(ixy) dy \quad (\text{A-54})$$

has been used in Eq. (A-52).

A.12 Ray Path Phase Delay

To compare wave theory and wave/optics results, it is helpful to have an expression for the phase delay along a ray. For a spherical symmetric

atmosphere, it follows from Eq. (A-1), Bouguer's law in Eq. (A-4a), and the bending-angle gradient in Eq. (A-5) that the phase delay between the emitting GPS satellite and the LEO is given by

$$\begin{aligned}
\varphi &= k \int n ds = k \int_{r_*}^{r_L} n \sqrt{1 + (r\theta')^2} dr + k \int_{r_*}^{r_G} n \sqrt{1 + (r\theta')^2} dr \\
&= k \int_{r_*}^{r_L} \frac{n^2 r dr}{\sqrt{n^2 r^2 - a^2}} + k \int_{r_*}^{r_G} \frac{n^2 r dr}{\sqrt{n^2 r^2 - a^2}} \\
&= \int_{\rho_*}^{\rho_L} \frac{\rho d\rho}{\sqrt{\rho^2 - \rho_*^2}} + \int_{\rho_*}^{\rho_G} \frac{\rho d\rho}{\sqrt{\rho^2 - \rho_*^2}} - 2 \int_{\rho_*}^{\infty} \frac{d \log n}{d\rho} \frac{\rho^2 d\rho}{\sqrt{\rho^2 - \rho_*^2}} \\
&= \sqrt{\rho_L^2 - \rho_*^2} + \sqrt{\rho_G^2 - \rho_*^2} + \rho_* \alpha_L(\rho_*) + \int_{\rho_*}^{\infty} \alpha_L(\omega) d\omega
\end{aligned} \tag{A-55}$$

where $\rho = nkr$ and $\rho_* = kn(r_*)r_* = ka$. We have assumed here that $d \log n / d\rho \rightarrow 0$ as $\rho \rightarrow \infty$.

Referring to Fig. A-3, the sides and angles of triangle OLG are completely determined from the precision orbit determination information, independent of the ray bending. This figure shows the ray asymptotes passing through the satellite positions G and L. These asymptotes are defined by the unit tangent vectors, \mathbf{T}_G and \mathbf{T}_L ; their deflection angles, δ_G and δ_L , with $\alpha = \delta_G + \delta_L$; and their impact parameter, a , or ρ_* in phase units. The value of the impact parameter is the same for both asymptotes when spherical symmetry applies. Therefore, the phase delay in Eq. (A-55) can be written as

$$\left. \begin{aligned}
\varphi &= \rho_G \cos(\chi_G + \delta_G) + \rho_L \cos(\chi_L + \delta_L) + \rho_* \alpha_L + \int_{\rho_*}^{\infty} \alpha_L(\omega) d\omega \\
\alpha_L &= \delta_L + \delta_G
\end{aligned} \right\} \tag{A-56}$$

Here χ_G and χ_L are strictly orbit-related angles. When $d \log n / d\rho \equiv 0$, $\delta_G = \delta_L = \alpha_L \equiv 0$ and $\rho_* \rightarrow \rho_L \sin \chi_L = \rho_G \sin \chi_G$. The phase delay is just $\rho_G \cos \chi_G + \rho_L \cos \chi_L = \rho_{LG}$. Thus, $\varphi - \rho_{LG}$ is the excess phase delay from the refracting atmosphere.

For the special case of when the emitting GPS satellite is placed at infinity with $\theta_G = \pi$, then from Fig. A-3 it follows that $\delta_G + \chi_G \rightarrow 0$, $\chi_L + \delta_L \rightarrow \theta_L + \alpha_L$, and $\rho_{LG} \rightarrow \rho_G + \rho_L \cos \theta_L$. The phase relative to the line $\theta = \pi/2$ becomes

$$\varphi = \rho_L \cos(\theta_L + \alpha_L) + \rho_* \alpha_L + \int_{\rho_*}^{\infty} \alpha_L(\omega) d\omega \tag{A-57}$$

References

- [1] J. Mathews and R. Walker, *Mathematical Methods of Physics*, Menlo Park, California: The Benjamin/Cummings Publishing Co., 1970.
- [2] C. Cartheodory, *Calculus of Variations and Partial Differential Equations of the First Order*, Part 2: Calculus of Variation, San Francisco: Holden-Day, Inc., 1967.
- [3] L. Pars, *An Introduction to the Calculus of Variations*, New York: John Wiley, 1962.
- [4] T. D. Moyer, *Formulation for Observed and Computed Values of Deep Space Network Data Types for Navigation*, New York: John Wiley, 2003.
- [5] I. Gelfand and S. Fomin, *Calculus of Variations*, Englewood Cliffs, New Jersey: Prentice-Hall, 1963.
- [6] M. E. Gorbunov, "Canonical Transform Method for Processing Radio Occultation Data in the Lower Troposphere," *Radio Science*, vol. 37, no. 5, 1076, doi:10.1029/2000RS002592, 2002.
- [7] J. Goodman, *Introduction to Fourier Optics*, New York: McGraw-Hill, 1968.
- [8] M. Born and E. Wolf, *Principles of Optics*, 6th ed., Oxford, United Kingdom: Pergamon Press, 1980.
- [9] E. Karayel and D. Hinson, "Sub-Fresnel Scale Vertical Resolution in Atmospheric Profiles from Radio Occultation," *Radio Science*, vol. 32, no. 2, pp. 411–423, 1997.
- [10] M. E. Gorbunov, A. S. Gurvich, and L. Bengtsson, *Advanced Algorithms of Inversion of GPS/MET Satellite Data and Their Application to Reconstruction of Temperature and Humidity*, Report 211, Max Planck Institute for Meteorology, Hamburg, Germany, 1996.
- [11] R. Phinney and D. Anderson, "On the Radio Occultation Method for Studying Planetary Atmospheres," *Journal of Geophysical Research*, vol. 73, no. 5, pp. 1819–1827, 1968.
- [12] W. G. Melbourne, E. S. Davis, C. B. Duncan, G. A. Hajj, K. R. Hardy, E. R. Kursinski, T. K. Meehan, L. E. Young, and T. P. Yunck, *The Application of Spaceborne GPS to Atmospheric Limb Sounding and Global Change Monitoring*, JPL Publication 94-18, Jet Propulsion Laboratory, Pasadena, California, April 1994.